Biosensors and Bioelectronics 47 (2013) 385–390

Contents lists available at SciVerse ScienceDirect

Biosensors and Bioelectronics

journal homepage: www.elsevier.com/locate/bios

An enzymatic biosensor for hydrogen peroxide based on CeO_2 nanostructure electrodeposited on ITO surface

Ajay Kumar Yagati [a], Taek Lee [b], Junhong Min [c,*], Jeong-Woo Choi [a,b,**]

[a] Research Center for Integrated Biotechnology, Sogang University, 35 Baekbeom-ro (Sinsu-dong), Mapo-gu, Seoul 121-742, Republic of Korea
[b] Department of Chemical and Biomolecular Engineering, Sogang University, 35 Baekbeom-ro (Sinsu-dong), Mapo-gu, Seoul 121-742, Republic of Korea
[c] School of Integrative Engineering, Chung-Ang University, Heukseok-dong, Dongjak-gu, Seoul 156-756, Republic of Korea

ARTICLE INFO

Article history:
Received 16 December 2012
Received in revised form
2 March 2013
Accepted 14 March 2013
Available online 26 March 2013

Keywords:
Electrodeposition
Cerium oxide
Electrochemistry
Myoglobin
Biosensor
Hydrogen peroxide

ABSTRACT

In this study, an enzymatic biosensor for amperometric detection of hydrogen peroxide was developed based on the direct electrochemistry of myoglobin (Mb) on a porous cerium dioxide (CeO_2) nanostructured film. The developed film accomplished with large surface area was electrodeposited on an indium tin oxide (ITO) substrate. Surface morphological studies revealed that the formed CeO_2 film has a large specific surface area with a unique nanostructure on the ITO surface. Cyclic voltammetry (CV) and differential pulse voltammetry (DPV) were employed to demonstrate the electrochemical behavior of Mb immobilized on the fabricated film, which exhibited facile, direct electrochemistry and good electrocatalytic performance without any electron mediator. The electrode displayed a pair of quasi-reversible reduction–oxidation peaks at −0.3 and −0.2 V, respectively, due to the Mb [Fe^{3+}/Fe^{2+}] redox couple, which is a surface-controlled electrochemical process with one electron transfer. This reagent-less biosensor showed good stability and high sensitivity for detecting H_2O_2 without any influence of intermediate compounds. This protein-based biosensor was capable of detecting H_2O_2 as low as 0.6 μM with linearity up to 3 mM and a response time of ~8 s, compared to those of other modified electrodes. Hence, porous CeO_2 is a possible candidate material for fabricating enzymatic sensors or devices.

1. Introduction

There is an increasing interest in the development of electrochemical biosensors based on biomolecules due to their potential applications in the field of clinical, environmental, and food industry-related samples due to their high sensitivity, selectivity, fast response, and low-cost (Hocevar et al., 2007; Shu et al., 2007; Yagati et al., 2011). Biomolecules having size matching the scale of nanomaterials have several advantages such as the ability to control, monitor and study biomolecular interactions (recognition, binding, and catalysis) for the design of efficient biosensing methods (Douvas et al., 2002; Pillet et al., 2013; Shih, 2008). The direct electrochemistry of redox proteins has received considerable attention in order to elucidate the intrinsic thermodynamic and kinetic properties of proteins and its potential application toward bioelectronic devices (Shi et al., 2009; Zheng et al., 2008). However, the proteins exhibit a rather slow rate of heterogeneous electron-transfer at conventional electrodes, because of deep burying of the electroactive prosthetic groups, the adsorptive denaturation of proteins onto electrodes and the unfavorable orientations at electrodes, although their electron-transfer is quite fast in biological systems (Armstrong, 2005; Thudi et al., 2012). Efforts have been made toward exploring new support materials and suitable methods to immobilize proteins on an electrode surface to obtain their direct electrochemical reactions and achieve a highly sensitive, selective, and durable electrochemical biosensor. An electron mediator, a small and diffusive redox species, is often required to facilitate communication between the protein redox center and the electrode surface (Cui et al., 2007; Zang et al., 2007). Alternatively, a mediator-less biosensor is a chemically modified electrode (CME) which itself provides an electron mediating function to facilitate direct electron transfer (Liu et al., 2005; Gooding et al., 2003). CMEs manufactured with porous materials have been widely applied to study direct electron transfer of proteins, due to their unique properties such as high surface area, good biocompatibility, and nontoxicity (Dai et al., 2004; Walcarius, 2001). Porous materials provide favorable microenvironments for proteins and enhanced electron transfer between the electro-active centers of the proteins and the electrode surface.

Nanostructured thin metal oxide films have received attention due to their unique morphology, grain size, porosity, and their

* Corresponding author. Tel.: +82 2 705 8480; fax: +82 2 3273 0331.
** Corresponding author at: Department of Chemical and Biomolecular Engineering, Sogang University, 35 Baekbeom-ro (Sinsu-dong), Mapo-gu, Seoul 121-742, Republic of Korea.
E-mail addresses: junmin@cau.ac.kr (J. Min), jwchoi@sogang.ac.kr (J.-W. Choi).

0956-5663/$ - see front matter © 2013 Elsevier B.V. All rights reserved.
http://dx.doi.org/10.1016/j.bios.2013.03.035

physical, electrical, and magnetic properties for applications in various fields including catalysis, gas sensing and separation, power storage and generation, and biology and medicine. The functional properties of nanoscopic metal oxide films have been recently highlighted in different areas, such as photovoltaic cells (Regan and Gratzel, 1991), gas sensors (Dittrich et al., 1999) and biosensors (Boyan et al., 1996). Many efforts have been made to synthesize, characterize and apply uniform porous materials over the last decade, due to their attractive textural and structural features, e.g., highly ordered structure, ultrahigh surface area, pore size distribution in the mesopore range, tunable pore sizes, and pore structures. Progress has been made in structural, compositional, and morphological control and the stability of porous materials for their emerging applications in catalysis, adsorption, and in sensing (Song et al., 2010; Ko et al., 2009).

An approach based on the use of nanostructured materials for a sensor application has been demonstrated to be promising and effective. TiO_2 (Zheng et al., 2008), MnO_2, (Yang and Hu, 2010), Fe_3O_4, (Yang et al., 2011), ZnO, (Zhu et al., 2007) and other similar nanostructured films have been used to assemble a new generation of biosensors for detecting H_2O_2 and also biological compounds such as 3,4-dihydroxyphenylacetic acid, ascorbic acid, guanine, L-tyrosine, acetaminophen, and β-NADH (Curulli et al., 2005). In our previous research we proposed some techniques to detect the biological materials (Kang et al., 2009; Choi et al., 2005; Choi et al., 2006) and bioelectronic device with simple function (Lee et al., 2010; Yagati et al., 2013). However, direct electrochemistry of proteins on this metal oxide film deposited electrode has not been reported yet.

In this study, cerium oxide (CeO_2) film is electrodeposited on an indium tin oxide (ITO) surface for direct electrochemistry of myoglobin (Mb) and to examine the electrocatalytic activity toward hydrogen peroxide. The fabricated film was analyzed by using scanning electron microscopy (SEM) and atomic force microscopy (AFM). Further, the electrochemical behavior of Mb/CeO_2/ITO electrode and sensing of H_2O_2 were established with electrochemical measurements.

2. Experimental details

2.1. Materials

Myoglobin (Mb) from horse heart was purchased from Sigma-Aldrich (St. Louis, MO, USA) and used as received without any further purification. Cerium (III) nitrate hexahydrate ($Ce(NO_3)_3 \cdot 6H_2O$) (99% pure), and Nafion perfluorinated resin solution (20 wt%), in a mixture of lower aliphatic alcohols and water, were purchased from Sigma-Aldrich. Hydrogen peroxide was obtained from Daejung Materials and Chemicals (Gyeonggi-Do, Korea) and diluted in deionized (DI) water to prepare desired molar solutions. 10 mM PBS buffer solution (pH 7.0) was used for all electrochemical experiments. All other solutions were prepared with DI water (18 MΩcm), which is purified using a Milli-Q system (Millipore, Bedford, MA, USA) (Choi et al., 2009; Lee et al., 2011).

2.2. Electrode cleaning procedure

ITO (20 Ω/cm^2) coated glass plate with a thickness of 400 nm was used. The transparent electrode was cleaned with an ultrasound in successive solutions of Triton X-100/water (1:5, v/v), water, and ethanol for at least 40 min each. The ITO electrode was then heated in a 1:1:5 solution of NH_4OH:H_2O_2:H_2O for 40 min at 80 °C, rinsed thoroughly with water, and dried under a stream of nitrogen gas.

2.3. Electrocathodic deposition of the CeO_2 film and immobilization of Mb on the fabricated surface

Electrochemical bath composed of 0.01, 0.1, and 0.2M Ce$(NO_3)_3 \cdot 6H_2O$ solutions were prepared at room temperature. The CeO_2 film was electrochemically deposited using a CHI 660A electrochemical workstation. The electrochemical deposition was carried out in a three-electrode cell using ITO as the working electrode, and a platinum wire and Ag/AgCl electrode were used as counter and reference electrodes, respectively. Deposition voltage was varied from −0.6 V to −1.8 V against the reference electrode at room temperature. After each deposition, the resultant films were washed with DI water and dried under N_2 stream.

A suspension (20 μL) of 0.1 mg/mL of Mb was cast onto the surface of the CeO_2/ITO electrode and maintained for 6 h to evaporate the water content, resulting in a uniform film. Then, 10 μL of 0.1 wt% Nafion solution was drop coated and dried at 4 °C. Nafion film is a commonly used film material in chemically modified electrodes for its unique ion-exchange, discrimination, chemical resistance, and biocompatible properties (Maensiri et al., 2007). For comparison studies, Mb/ITO electrode was prepared using bare ITO instead of deposited CeO_2. After immobilizing the electrodes overnight at 4 °C, it was rinsed with distilled water and dried under N_2 stream. The dried electrodes were stored at 4 °C when not in use.

2.4. Characterization of the fabricated film on the ITO surface

The surface topography of bare and deposited films on the ITO surface was confirmed with SEM measurements using a JEOL JSM S-4300 microscope at an operating voltage of 20 kV. AFM images were obtained using Nanoscope IV/Multimode (Digital Instruments (Tonawanda, NY, USA). All AFM images were recorded in tapping mode using a silicon cantilever with resonance frequencies (f_o) of 250–300 kHz. The X-ray diffraction (XRD) patterns of the prepared samples were recorded with Cu Kα radiation (λ) of 1.54056 Å from a Rigaku X-ray diffractometer at a scanning rate of 0.02 °/second in 2θ. The X-ray diffractometer was operated at 40 kV and 150 mA. Optical measurements were conducted using a JASCO-V-660 spectrophotometer. The dimensions of the substrates were 20 × 20 mm^2. A bare ITO substrate was used as the reference sample.

2.5. Electrochemical activity and H_2O_2 detection

Cyclic voltammetry (CV) and linear sweep voltammetry (LSV) was performed with a three-electrode system using the Mb/CeO_2/ITO substrate as the working electrode, a platinum wire as the counter electrode, and Ag/AgCl/KCl_{sat} as the reference electrode. Experiments were performed using a CHI 660A potentiostat equipped with general purpose electrochemical software. Amperometric (I/t) and DPV measurements were performed on the Mb/CeO_2/ITO electrode using various H_2O_2 concentrations. The potential was set at −0.30 V, and the current–time curves were recorded after successive additions of 10 μL of 100 mM H_2O_2 in 5 mL of 10 mM PBS (pH 7.0) buffer. Convective transport during amperometric determination was achieved with magnetic stirring at 600 rpm. The buffer solution was purged with highly purified nitrogen throughout the experiment.

3. Results and discussion

3.1. Formation and optimization of metal oxide film on the ITO surface

Electrocathodic deposition of the CeO_2 porous film was performed with cyclic voltammetry using different working

electrodes immersed in increasing concentrations (0.01, 0.1, and 0.2 M) of fresh cerium nitrate solutions in the potential range of −0.6 V to −1.8 V vs. Ag/AgCl/KCl_{sat}. As shown in Fig. 1, the hysteresis of the reverse scan indicated that the metal oxide film was deposited on the ITO surface. Additionally, the hysteresis and the current densities increased with an increase in the cerium nitrate solution concentration. To optimize the metal oxide content to develop a sensitive amperometric sensor, electrode performance after protein immobilization was optimized with respect to metal oxide loading in terms of the depositing concentration that produced a higher amperometric response. Biosensors containing different CeO_2 concentrations were fabricated and tested for this purpose while maintaining the Mb amount in the immobilization matrix constant. A higher amperometric response was obtained with a 0.1M CeO_2 film. Increasing the CeO_2 concentration did not result in a higher current intensity. Fig. S1 shows the SEM images obtained for various concentrations (0.01, 0.1, and 0.2 M) under identical conditions on the ITO surface. It was clearly observed that the deposited film appeared to be like cerium nanoparticles at lower concentrations and the grain size increased with increasing concentrations of cerium nitrate solution leading to a porous structure.

3.2. Confirmation of protein immobilization on the fabricated surface

The formation of the cerium oxide film and further deposition of Mb on the fabricated surfaces were characterized with SEM (Fig. 2a–c) and AFM analysis (Fig. S2, Supporting Information). Both the analyses revealed that the electrodeposition of CeO_2 film was well formed on the ITO surface. The ITO surface showed ridges all over the surface compared to that of the deposited film, which showed rough fragments possessing a well-defined three-dimensional structure over the entire surface. Nucleation of the oxides from the precursor solution occurred at the molecular level, and the films had uniform and dense microstructures. Furthermore, the rough structure was adsorbed with protein molecules that formed a smoother surface when the protein and nafion were immobilized (Fig. 2c). Also, AFM analysis clearly showed the adsorbed molecules on the surface as the Mb was well adsorbed on the CeO_2/ITO surface.

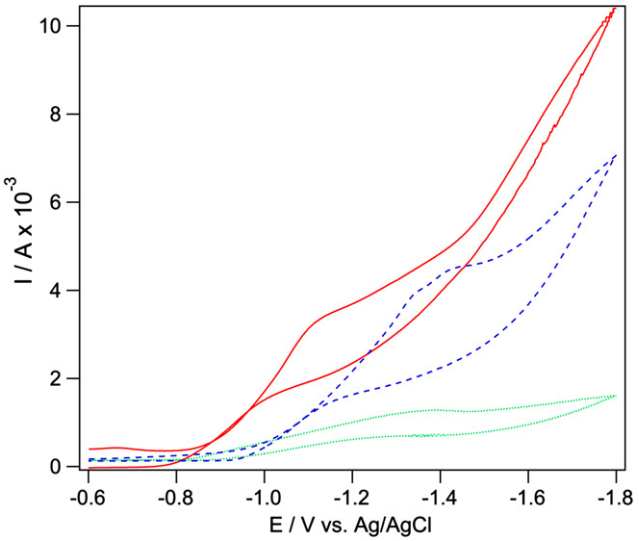

Fig. 1. Cyclic voltammograms represent the electrocathodic deposition of cerium nanostructured film on ITO surface of (···) 0.01 M, (---) 0.1 M and (—) a 0.2 M solutions at a scan rate of 50 mV s^{-1}.

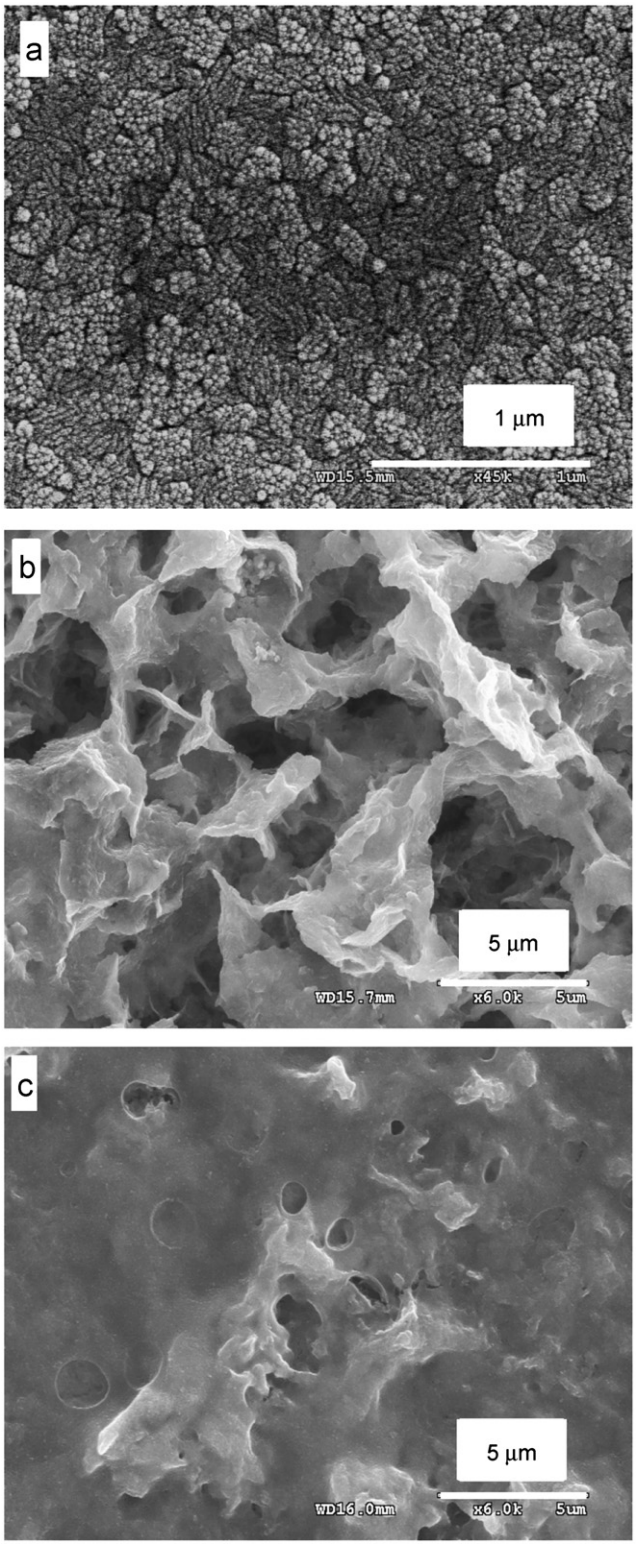

Fig. 2. SEM images of (a) bare ITO surface, (b) electrodeposited cerium film on ITO and (c) myoglobin immobilized on cerium oxide film ITO surface.

3.3. UV–vis and XRD analysis of the CeO_2/ITO electrode surface

The UV spectra of the bare ITO showed an absorption peak at 550 nm which is typical for an ITO surface, and the absorption edge for CeO_2/ITO from the spectrum was observed at 360 nm (Fig. 3a and b). A previous study indicated that CeO_2/ITO reveals an

absorption band in the wavelength region of 270–400 nm, which is assigned to the charge transfer transition from the $O^{2-}(2p)$ to Ce^{4+} (4f) orbital in CeO_2 (Ansari et al., 2009a). Additionally, Fig. 3c shows the results of XRD studies carried out on the nanostructured CeO_2 film deposited on the ITO substrate. The XRD pattern results indicated that the CeO_2 film was crystalline and had diffraction peaks corresponding to (1 1 1), (2 0 0), (2 2 0), and (3 1 1) planes, which could be indexed to the pure cubic fluorite structure of CeO_2. The intensities and positions of the peaks agreed with the literature (JCPDS card, no. 4-0593). It was also shown that the ITO surface resolved the XRD peaks corresponding to the (2 1 1), (2 2 2), (4 0 0), (4 1 1), (4 3 1), and (4 4 0) planes. The intensities and positions of the peaks agreed with the JCPDS card file (JCPDS file: 01-088-2160) (Yagati et al., 2012).

3.4. Electrochemical behavior of the CeO_2/ITO and Mb/CeO_2/ITO electrodes

The CVs for both CeO_2/ITO and bare ITO electrodes are depicted in Fig S3a. No obvious redox peaks were observed for bare ITO electrode, whereas well-defined reversible redox peaks (E_{pa}=0.6 V and E_{pc}=0.3 V) appeared on electrodeposited CeO_2-modified electrode in 10 mM PBS solution. These peaks were due to formation of Ce^{3+}/Ce^{4+} couple. These results further confirmed the formation of CeO_2 on the surface of the ITO electrode and demonstrate an excellent electrochemical nature of the film. Fig. S3b shows the CVs of CeO_2/ITO at different scan rates in pH 7.0 PBS. A pair of roughly symmetric redox peaks appearing with almost equal heights to the redox peak currents at scan rates 0.01–0.1 mVs^{-1} was observed. A good linear relationship between the redox peak current and the scan rate with results of I_{pc} (μA)=(0.0071) (mV s^{-1})+0.3597 (R^2=0.9931) and I_{pa} (μA)=(−0.0062) (mV s^{-1}) −0.5309 (R^2=0.9952) was observed. Such behavior revealed that the electron transfer between CeO_2 film and ITO was a surface-controlled electrochemical process. Fig. 4 shows the direct electrochemistry of Mb immobilized on the CeO_2/ITO electrode surface in 10 mM PBS. It can be clearly seen that two pairs of quasi-reversible reduction and oxidation peaks were observed, which corresponded to CeO_2 and Mb. The peaks at −0.38 and −0.2 V corresponded to the Fe^{3+}/Fe^{2+} redox center of Mb. The formal potential ($E^{0'}$), for Mb, calculated from the midpoint of the reduction and oxidation peak potentials, was −290 mV (vs. Ag/AgCl), and the peak-to-peak potential difference (ΔE_p) was 180 mV. These results confirmed that Mb on CeO_2/ITO electrode displayed a quasi-reversible electrochemical reaction. Scan rate analysis on Mb/CeO_2/ITO electrode was performed in 10 mM PBS pH 7.0 from 20 to 200 mVs^{-1} range (Fig. S3c). Results show that both cathodic and anodic peak currents were almost symmetrical and linearly proportional to square root of scan rate ($\nu^{1/2}$) in the range of 0.02–0.2 mVs^{-1}, suggesting a typical diffusion controlled process. The regression equations were $I_{pc}=0.1449\,\nu^{1/2}-0.528$ (μA, Vs^{-1}, R^2=0.982) and $I_{pa}=-0.138\nu^{1/2}+0.487$ (μA, V s^{-1}, R^2=0.983). A graph of $E_p=f$ (log ν) yielded two straight lines with slopes of $-2.3RT/\alpha nF$ and $2.3RT/(1-\alpha)nF$ for the cathodic peak and anodic peak, respectively (Fig. S4a and b). Thus, the value of α was estimated to be 0.533 from the slopes of the straight lines based on the following equation (Tian et al., 2009):

$$\log\frac{\nu_a}{\nu_c}=\log\frac{\alpha}{1-\alpha} \quad (1)$$

The following Laviron equation was used to calculate the value of the apparent heterogeneous electron transfer rate constant (k_s):

$$\log k_s=\alpha\log(1-\alpha)+(1-\alpha)\log\alpha-\log\frac{RT}{nF\nu}-\frac{\alpha(1-\alpha)nF\Delta E_p}{2.3RT} \quad (2)$$

where α is the electron transfer coefficient, n is the number of electrons, ΔE_p is the separation of the redox peaks, and ν is the scan rate. The electron transfer rate constant (K_s) was calculated to be 1.57 s^{-1}.

According to the Laviron equation (Laviron, 1979), $I_p=n^2F^2A\Gamma\nu/4RT$, the surface coverage (Γ) of Mb immobilized on the surface of the CeO_2/ITO modified electrode was 5.142 × 10−11 mol cm^{-2}, indicating that several layers of Mb were entrapped in the composite film and participated in the electron transfer process.

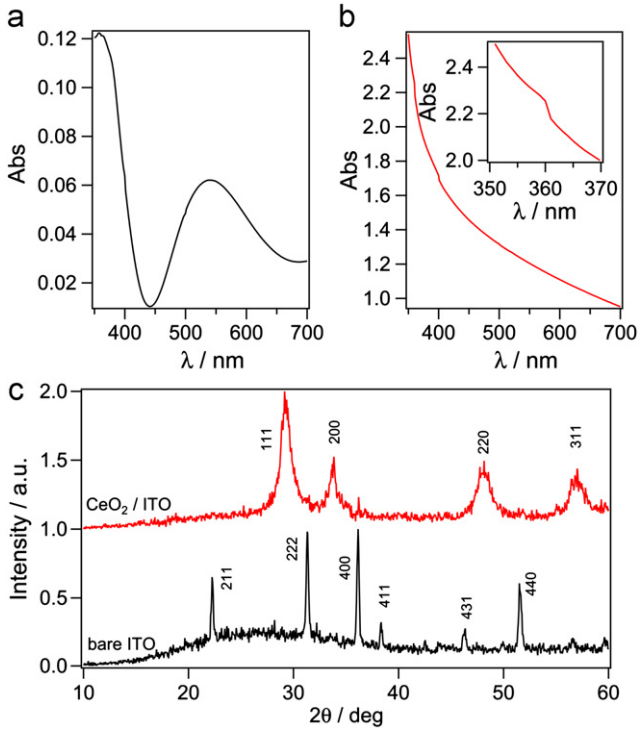

Fig. 3. UV–vis absorption spectra obtained for (a) bare ITO; (b) cerium oxide on ITO surface; *inset* shows the zoomed portion of the image in the range of 350–370 nm; and (c) XRD patterns for bare and cerium oxide deposited film on ITO surface.

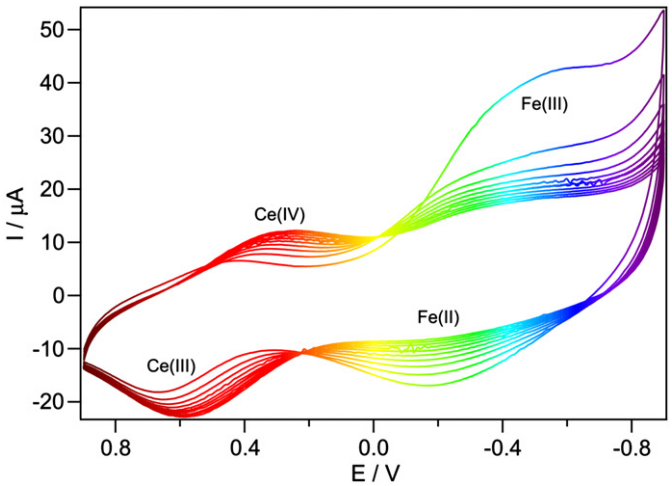

Fig. 4. Cyclic voltammograms obtained from Mb/CeO_2/ITO electrode in a wide potential range showing redox properties of both CeO_2 and Mb layers on ITO surface.

3.5. Analytical performance of the Mb/CeO_2/ITO electrode for detecting H_2O_2

DPV and LSV were recorded in 10 mM PBS to further probe into the electrochemical behavior of Mb/CeO_2/ITO and its individual components. Fig. 5a shows the DPV of Mb/CeO_2/ITO recorded by a potential sweep between −0.15 and 0.20 V (vs. Ag/AgCl) where clear reduction peaks were attributed to the reduction of both CeO_2 and Mb, which was observed at 0.10 and −0.075 V respectively. Additionally, Fig. S5 and b shows that the DPV of CeO_2/ITO and Mb/ITO electrodes had peak potentials at −0.05 V and −0.125 V, respectively, where a small change in peak potential distribution compared to that of hybrid structure occurred. This may be due to both redox materials in the same molecular environment or the surface confinement of the protein on the electrode surface that resulted in the shift in their redox potentials. Also, LSV clearly showed the formation of CeO_2/ITO, Mb/ITO, and Mb/CeO_2/ITO electrode surfaces, shown in Fig. S5c and d. DPV and amperometric (I/t) measurements were conducted on the Mb/CeO_2/ITO to elucidate the electrocatalytic response to H_2O_2.

The mechanism of the electrocatalytic reduction of H_2O_2 is expressed as

$$\text{Mb } (Fe^{3+}) + H_2O_2 \rightarrow \text{Intermediate I}(Fe^{4+}=O) + H_2O \quad (3)$$

$$\text{Intermediate I}(Fe^{4+}=O) + H^+ + e^- \rightarrow \text{Intermediate II} \quad (4)$$

$$\text{Intermediate II} + H^+ + e^- \rightarrow \text{Mb } (Fe^{3+}) + H_2O \quad (5)$$

DPV signals (Fig. 5b) were obtained after adding 10 μL aliquots of 100 mM H_2O_2 to the Mb/CeO_2/ITO in 10 mM PBS. Each addition of H_2O_2 clearly showed that the Mb/CeO_2/ITO electrode had a good electrocatalytic response to detect H_2O_2. We selected a potential of −0.15 V more negative than the reduction potential of Mb to completely reduce the test compound. Thus, an applied potential of −0.3 V was used to obtain the chronoamperometric response. The Mb/CeO_2/ITO electrode in PBS buffer solution was tested with different concentrations of H_2O_2 and then chronoamperogram was recorded with nitrogen purging to circumvent oxygen interference to obtain a calibration curve (Fig. 6a). A calibration plot *inset* (i) was obtained for different concentrations of H_2O_2 between 0.2 mM and 5 mM with a dynamic range up to 3 mM. The linear regression equation is expressed as follows: I_p (μA) = 13.54[H_2O_2 mM] + 6.33, with an R^2 value of 0.9825. The sensitivity of the Mb/CeO_2/ITO electrode toward H_2O_2 was 5.4 μA mM^{-1} cm^{-2}, and the detection limit of H_2O_2 was 0.6 μM. This detection limit was lower than the value previously obtained for H_2O_2 and compared with other electrochemical methods shown in Table S1 (supplementary information). The inset (ii) shows the response current at a steady state after adding H_2O_2, in which 95% of the steady state current was achieved after about 10 s. The fabricated biosensor, which responded within 10 s, was considered acceptable for in vivo diagnostic applications (Ansari et al., 2009b).

A response plateau in the calibration curve was observed when the H_2O_2 concentration was > 3 mM, showing the characteristics of a Michaelis–Menten kinetic mechanism. A reflection of the

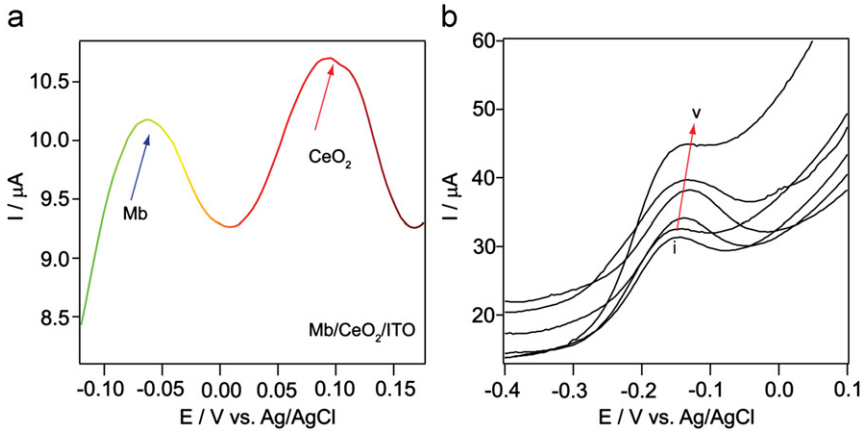

Fig. 5. Differential pulse voltammogram (DPV) for (a) Mb/CeO_2/ITO surface in 10 mM PBS at pH 7.0 shows both the myoglobin and cerium oxide distinct peaks. (b) DPV for Mb/CeO_2/ITO electrode as a function of H_2O_2 upon successive additions of 5 μL aliquots of 100 mM H_2O_2 in 5 mL solution of 10 mM PBS at pH 7.

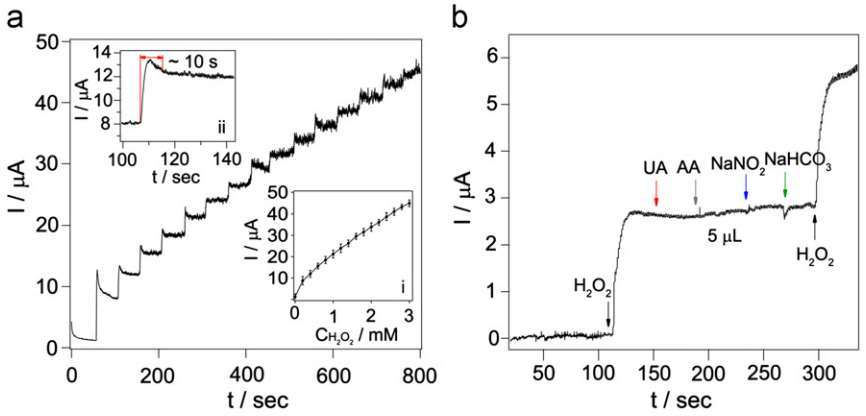

Fig. 6. (a) Amperometric (I/t) curve obtained for Mb/CeO_2/ITO electrode upon successive additions of 10 μL aliquots of 100 mM H_2O_2 to 5 mL of 10 mM PBS with constant stirring at an applied potential of −0.3 V under nitrogen purging. Inset figure (i) shows the calibration curve and (ii) shows the response time of Mb/CeO_2/ITO electrode toward the detection of H_2O_2. (b) I/t curve obtained for Mb/CeO_2/ITO electrode at −0.3 V upon successive additions of 5 μL aliquots of (0.2 mM) uric acid (UA), L-ascorbic acid (AA), sodium nitrite ($NaNO_2$) and sodium bicarbonate ($NaHCO_3$) along with 5 μL of H_2O_2 with constant stirring of 5 mL PBS buffer pH 7.0.

enzyme–substrate kinetics was calculated by the Lineweaver–Burk equation to obtain quantitative information on the effect of the metal oxide microenvironment on enzyme activity of the apparent Michaelis–Menten constant (K_m^{app}) (Mehta et al., 2007):

$$1/I_{ss} = 1/I_{max} + K_m^{app}/I_{max}C \quad (6)$$

where I_{ss} is the steady current obtained after adding substrate, C is the bulk concentration of the substrate, and I_{max} is the maximum current measured under the saturated substrate condition. The apparent Michaelis–Menten constant (K_m^{app}) was 3.15 mM, suggesting that the biosensor exhibited high affinity for H_2O_2.

Selectivity is also important during practical use of a biosensor. Ascorbic acid, uric acid, sodium nitrite and sodium bicarbonate were tested at 0.2 mM to evaluate electrode selectivity. The amperometric responses of the biosensor were obtained following consecutive injections of (0.2 mM) 5 μL H_2O_2 with the above interfering species (Fig. 6b). It was evident that there was minimal influence of interfering species on the H_2O_2 response. Injecting (0.2 mM) 5 μL H_2O_2 with 10 μL of the above interfering species resulted in a negligible response, indicating a high selective biosensor (Fig. S6). The stability of the Mb/CeO_2/ITO was examined by monitoring current response after successively cycling the modified electrode in the potential range of +0.3 to −0.25 V for several cycles. Additionally, reproducibility of this biosensor was studied in the linear range of H_2O_2. After a storage period of 1 week at 4 °C, the Mb/CeO_2/ITO electrode did not change its response to 10 mM H_2O_2 in pH 7.0 PBS. After 2 weeks, the sensor retained 95% of its initial response to H_2O_2. Thus, CeO_2 and Nafion played film-forming and adhesion roles to immobilize Mb. The relative standard deviation was 2.3% for six successive measurements of 3 mM H_2O_2 in 10 mM PBS (pH 7.0), showing that the proposed biosensor displayed acceptable reproducibility.

4. Conclusions

In summary, a CeO_2 film with high surface area was utilized to immobilize Mb as a modified ITO electrode. The electrodeposited CeO_2 provided electron transfer between the Mb and the underlying ITO surface to electrochemically detect H_2O_2. The electrochemical biosensor could measure H_2O_2 at a very low limit of detection (0.6 μM). The high sensitivity (5.4 μA mM^{-1} cm^{-2}) of the sensor might be attributed to the large surface area and enhanced electrocatalytic activity of the CeO_2-modified surface, with conductivity due to a metal oxide material, and a minimized background current level obtained by optimizing the process under various experimental conditions. Easy and simple fabrication, low cost, and excellent electrochemical catalysis with high selectivity were achieved for signal detection thereby avoiding conduction of complex detection steps. The developed platform offer the advantages of simplicity, efficiency and speed to evaluate a target, which is essential for developing user-friendly sensor platforms and could be used for sensitive and selective detection of other materials.

Acknowledgments

This research was supported by The Nano/Bio Science & Technology Program (M10536090001-05N3609-00110) of the Ministry of Education, Science and Technology (MEST), by the National Research Foundation of Korea (NRF) grant funded by the Korea government (MEST) (2009-0080860), and by the Ministry of Knowledge Economy (MKE) and Korea Institute for Advancement in Technology (KIAT) through the Workforce Development Program in Strategic Technology.

Appendix A. Supplementary Information

Supplementary data associated with this article can be found in the online version at http://dx.doi.org/10.1016/j.bios.2013.03.035.

References

Ansari, A.A., Sumana, G., Khan, R., Malhotra, B.D., 2009a. Journal for Nanoscience and Nanotechnology 9, 4679–4685.
Ansari, A.A., Solanki, P.R., Malhotra, B.D., 2009b. Journal of Biotechnology 142, 179–184.
Armstrong, F.A., 2005. Current Opinion in Chemical Biology 9, 110–117.
Boyan, B.D., Hummert, T.W., Dean, D.D., Schwartz, Z., 1996. Biomaterials 17, 137–146.
Choi, J.-W., Kim, J.S., Kim, S.-U., Min, J., 2009. Biochip Journal 3, 157–163.
Choi, J.-W., Lee, W., Oh, B.-K., Lee, H., Lee, D., 2006. Biosensors & Bioelectronics 22, 764–767.
Choi, J.-W., Park, K., Lee, D., Lee, W., Lee, W.H., 2005. Biosensors & Bioelectronics 20, 2300–2305.
Cui, X., Li, C.M., Zang, J., Yu, S., 2007. Biosensors & Bioelectronics 22, 3288–3292.
Curulli, A., Valentini, F., Padeletti, G., Viticoli, M., Caschera, D., Palleschi, G., 2005. Sensors and Actuators, B, 111, 441–449.
Dai, Z., Liu, S., Ju, H., Chen, H., 2004. Biosensors & Bioelectronics 19, 861–867.
Dittrich, T., Weidmann, J., Koch, F., 1999. Applied Physics Letters 75, 3980–3982.
Douvas, A., Argitis, P., Misiakos, K., Diotikali, D., Petrou, P.S., Kakabakos, S.E., 2002. Biosensors & Bioelectronics 17, 269–278.
Gooding, J.J., Wibowo, R., Liu, J., Yang, W., Losic, D., Orbons, S., Mearns, F.J., Shapter, J.G., Hibbert, D.B., 2003. Journal of the American Chemical Society 125, 9006–9007.
Hocevar, S.B., Svancara, I., Ogorevc, B., Vytras, K., 2007. Analytical Chemistry 79, 8639–8643.
Kang, D., Lee, J., Oh, B.-K., Choi, J.-W., 2009. Biosensors & Bioelectronics 24, 1431–1436.
Ko, H., Chang, S., Tsukruk, V.V., 2009. ACS Nano 3, 181–188.
Laviron, E., 1979. Journal of Electroanalytical Chemistry 100, 263–270.
Lee, T., Kim, S.-U., Min, J., Choi, J.-W., 2010. Advanced Materials 22, 510–514.
Lee, T., Min, J., Kim, S.-U., Choi, J.-W., 2011. Biomaterials 32, 3815–3821.
Liu, A., Wei, M., Honma, I., Zhou, H., 2005. Analytical Chemistry 77, 8068–8074.
Maensiri, S., Masingboon, C., Laokul, P., Jareonboon, W., Promarak, V., Anderson, P.L., Seraphin, S., 2007. Crystal, Growth and Design 7, 950–956.
Mehta, A., Patil, S., Bang, H., Cho, H.J., Seal, S., 2007. Sensors and Actuators A 134, 146–151.
Pillet, F., Sanchez, A., Formosa, C., Séverac, M., Trévisiol, E., Bouetd, J., Leberrea, V.A., 2013. Biosensors & Bioelectronics 43, 148–154.
Regan, B.O., Gratzel, M., 1991. Nature 353, 737–740.
Shi, L., Liu, X., Niu, W., Li, H., Han, S., Chen, J., Xu, G., 2009. Biosensors & Bioelectronics 24, 1159–1163.
Shih, W., 2008. Nature Materials 7, 98–100.
Shu, X., Chen, Y., Yuan, H., Gao, S., Xiao, D., 2007. Analytical Chemistry 79, 3695–3702.
Song, L., Feng, D., Fredin, N.J., Yager, K.G., Jones, R.L., Wu, Q., Zhao, D., Vogt, B.D., 2010. ACS Nano 4, 189–198.
Thudi, L., Jasti, L.S., Swarnalatha, Y., Fadnavis, N.W., Mulani, K., Deokar, S., Ponrathnam, S., 2012. Colloids and Surfaces B 90, 184–190.
Tian, F., Gourine, A.V., Huckstepp, R.T.R., Dale, N., 2009. Analytica Chimica Acta 645 (2009), 86–91.
Walcarius, A., 2001. Chemistry of Materials 13, 3351–3372.
Yagati, A.K., Lee, T., Min, J., Choi, J.-W., 2011. Bioelectrochemistry 80, 169–174.
Yagati, A.K., Lee, T., Min, J., Choi, J.-W., 2012. Colloids and Surfaces B 92, 161–167.
Yagati, A.K., Lee, T., Min, J., Choi, J.-W., 2013. Biosensors & Bioelectronics 40, 283–290.
Yang, J., Xiang, H., Shuai, L., Gunasekaran, S., 2011. Analytica Chimica Acta 708, 44–51.
Yang, Y.J., Hu, S., 2010. Electrochimica Acta 55, 3471–3476.
Zang, J., Li, C.M., Cui, X., Wang, J., Sun, X., Dong, H., Sun, C.Q., 2007. Electroanalysis 19, 1008–1014.
Zheng, W., Zheng, Y.F., Jin, K.W., Wang, N., 2008. Talanta 74, 1414–1419.
Zhu, X., Yuri, I., Gan, X., Suzuki, I., Li, G., 2007. Biosensors & Bioelectronics 22, 1600–1604.